NANO LETTERS

2007
Vol. 7, No. 9
2693−2700

Nanometer Positioning, Parallel Alignment, and Placement of Single Anisotropic Nanoparticles Using Hydrodynamic Forces in Cylindrical Droplets

Richa Sharma, Chang Young Lee, Jong Hyun Choi, Kejia Chen, and Michael S. Strano*

Department of Chemical Engineering, Massachusetts Institute of Technology, Cambridge, Massachusetts 02139

Received May 14, 2007; Revised Manuscript Received June 8, 2007

ABSTRACT

Droplets of liquid drying on a surface with pinned contact area develop an internal hydrodynamic flow that carries entrained particles to the air–liquid–substrate interface. We use this phenomenon in cylindrical, micrometer-sized droplets of large aspect ratio (more than 1000:1) to align, position, and place individual anisotropic nanostructures such as single-walled carbon nanotubes (SWNT). More than 84% of SWNT are aligned in parallel within ±5° relative to the target axis of alignment. A potential flow model accurately describes and quantifies the statistical variation in the positioning of the nanostructures. We demonstrate for the first time the top-down parallel alignment and placement of individual (unbundled) nanotubes from solution electrically contacted across gold electrodes.

Introduction and Motivation. An important, yet unresolved problem in nanotechnology is the large-scale, top-down placement of nanostructures from solution with controlled orientation, position, and adhesion to a surface. Such control is essential for advances in nanoelectronics,[1,2] sensor development,[3−6] and synthesis of photonic arrays.[7] A diverse set of approaches have been proposed including dielectrophoresis,[8,9] gas flow,[10] magnetic alignment,[11] electrospray,[12] quasi-two-dimensional nematic phases,[13] and self-assembled monolayers (SAMs) with high affinity for nanoparticles[14−16] assembled via microcontact printing or dip-pen nanolithography. Only the last two techniques are capable of aligning and trapping anisotropic nanoparticles without an externally applied force. The approach using nematic phases does not give uniform alignment on a large scale as the angle of alignment varies spatially with the distance from the electrodes. Moreover, this technique uses DNA-coated nanotubes,[17] where adsorbed DNA is difficult to be removed after deposition on a surface. Similarly, the approaches using SAMs require a specific surface chemistry or its absence on the nanoparticle that interacts with the patterned layers on the surface. This is problematic when incompatible chemistries are needed to disperse nanoparticles in solution, as is typically the case. As an example, these methods have only been utilized to align and place less-useful bundles (aggregates) of SWNT because organic solvents are required for the deposition.[18] The requirement of a particular surface chemistry also confounds the ability to functionalize and treat nanoparticles before assembling them on a surface. The absence of an efficient technique has led to an increased interest in CVD[19,20] grown SWNT directly on substrates rather than on bulk grown SWNT.

Several researchers have utilized evaporating droplets to assemble nanoparticles such as SWNT,[21] but it is not obvious that such approaches can yield precision of single-particle deposition. Additionally, the spherical geometries of the droplets utilized are less advantageous, confining materials to circular or ring-shaped patterns that are not easily incorporated into complex electrical devices, such as field effect transistors and metallic interconnect applications, for which parallel alignment of single nanotubes and bundles[22] of nanotubes is respectively desired.

Picknett and Bexon[23] distinguished between two modes of evaporation of sessile drops on solid surfaces. In one, the contact angle remains constant and the contact area decreases, which is also called *depinned contact* or *shrinking*. In the second mode the contact area is constant with decreasing contact angle, known as *pinned contact*. The nature of the contact lines during evaporation is a function of several

* Corresponding author. E-mail: strano@mit.edu.

10.1021/nl0711211 CCC: $37.00
Published on Web 08/04/2007

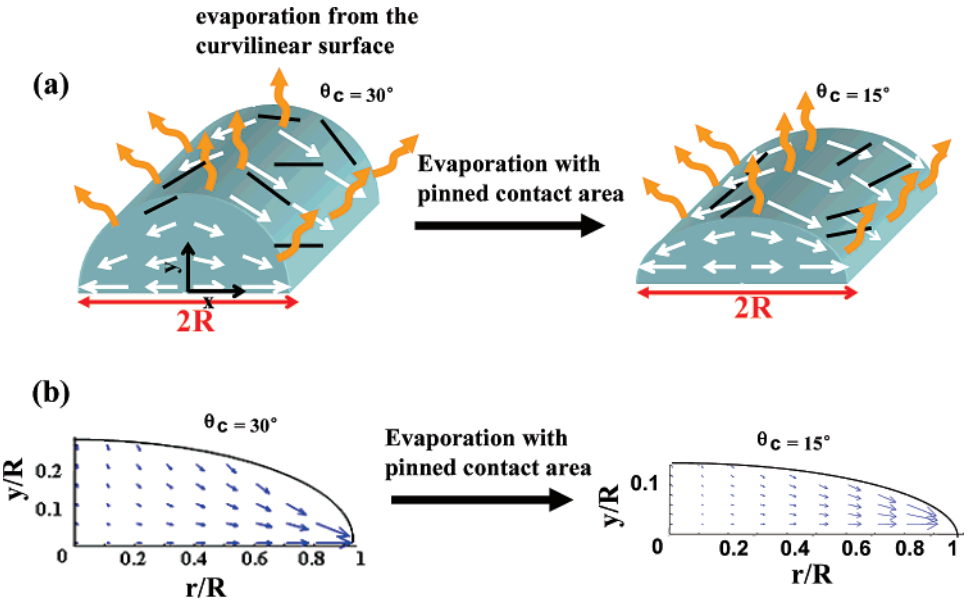

Figure 1. Hydrodynamics in a cylindrical drop to align and place anisotropic nanoparticles. (a) Solvent evaporating from the curvilinear surface of a cylindrical droplet with constant, pinned contact area and decreasing contact angle from 30° to 15°. White arrows represent the internal flow field in the droplet that carry entrained particles (black rods representing the anisotropic nanoparticles (SWNT)) to the outer edges of the droplet. (b) Velocity vector field in the cylindrical droplet drying with pinned contact area and decreasing contact angle from 30° to 15°. (Note: *y*-axis is not in scale with the *x*-axis)

factors, including the rheological properties of the evaporating liquid, surface roughness and heterogeneity, the rate of the evaporation, and the evaporation mechanism. As observed by several researchers, evaporation may be by only one of the above modes[24,25] or by a third mode that is a combination of the first two modes, particularly pinned contact drying followed by shrinkage drying.[26,27] Many believe that the origin of the third mode (evaporation mode switching) is the existence of contact angle hysteresis[23] on a surface.[26] Accordingly, the hysteresis leads to an evaporation mode initially with an unchanged contact area and a diminishing contact angle until the receding contact angle is attained. After this, the constant contact angle (depinned contact) mode supersedes.[26,27]

Degan et al.[28,29] and Petsi and Burganos[30,31] have investigated the flow pattern inside drying droplets with both spherical and cylindrical geometry. Pinning of the contact line of the drying droplet ensures that liquid evaporating from the edges is replenished by liquid from the interior. This leads to an internal flow toward the contact line. Hence pinned contact drying of droplets of colloidal suspensions forms "coffee ring" stains[28] due to this internal flow carrying all the suspended particles toward the edges of the droplet. This phenomenon of ring-type deposition resulting from droplet drying with pinned contact has successfully been used to assemble diblock copolymers,[32] DNA,[33] gold nanocrystals,[34] and aligned mesh of carbon nanotubes on various surfaces.[21]

An unanswered question is whether the internal hydrodynamics of a drying cylindrical droplet can align, place, and deposit individual anisotropic nanoparticles such as nanotubes or nanowires with precision on a nanometer scale. In this work, we explore this possibility and its potential applications.

Concept and Mathematical Development. When a solvent evaporates at a constant, pinned contact area from a cylindrical droplet (Figure 1a), an internal flow develops (Figure 1b) similar to the case of spherical droplets.[28,29] Entrained particles are expected to be carried to the outer edges of the droplet due to this flow. Petsi and Burganos[31] derived an analytical solution for the potential flow inside this evaporating cylindrical droplet. The potential flow in the droplet follows $\nabla^2\varphi = 0$ (irrotational and incompressible flow), with the velocity potential described by $v = \nabla\varphi$, where φ and v are velocity potential and velocity, respectively. Using a bipolar coordinate system, they showed that the resulting velocity components in Cartesian coordinates are:

$$v_x(\alpha,\beta) = \frac{\cosh\alpha\cos\beta + 1}{\cosh\alpha + \cos\beta}v_\alpha + \frac{\sinh\alpha\sin\beta}{\cosh\alpha + \cos\beta}v_\beta \quad (1a)$$

$$v_y(\alpha,\beta) = -\frac{\sinh\alpha\sin\beta}{\cosh\alpha + \cos\beta}v_\alpha + \frac{\cosh\alpha\cos\beta + 1}{\cosh\alpha + \cos\beta}v_\beta \quad (1b)$$

where the velocity components in a bipolar coordinate system (α,β,z)[31]are:

$$v_\alpha(\alpha,\beta) = -\frac{2}{\pi}(\cosh\alpha + \cos\beta)\int_0^\infty \frac{\cosh\lambda\beta\sin\lambda\alpha}{\sinh\lambda\theta_c(t)} \times \left[\int_0^\infty \frac{(u_{ns} + J/\rho)\cos\lambda a'}{\cosh a' + \cos\theta_c(t)}\,da'\right]d\lambda \quad (2a)$$

$$v_\beta(\alpha,\beta) = \frac{2}{\pi}(\cosh\alpha + \cos\beta)\int_0^\infty \frac{\sinh\lambda\beta\cos\lambda\alpha}{\sinh\lambda\theta_c(t)} \times \left[\int_0^\infty \frac{(u_{ns} + J/\rho)\cos\lambda a'}{\cosh a' + \cos\theta_c(t)}\,da'\right]d\lambda \quad (2b)$$

Here, J is the local evaporation flux, $\theta_c(t)$ is the contact angle

at time t, ρ is the liquid density, and $u_{ns}(t)$ is the normal component of the surface velocity at time t given by:

$$u_{ns}(t) = \frac{J_o}{\rho} \frac{\theta_c(t)}{\sin \theta_c(t) - \theta_c(t) \cos \theta_c(t)} \times \left(\cos \theta_c(t) - \sqrt{1 - \left(\frac{x}{R}\right)^2 \sin^2 \theta_c(t)}\right) \quad (3)$$

J is assumed to be constant over the surface of the droplet and equal to J_o. Both $u_{ns}(t)$ and $\theta_c(t)$ are functions of time, and for a constant contact area evaporation, the contact angle decreases with time as:

$$\frac{d\theta_c(t)}{dt} = \frac{J_{TOT}(t)}{2\rho R^2} \frac{\sin^3 \theta_c(t)}{\sin \theta_c(t) - \theta_c(t) \cos \theta_c(t)} \quad (4)$$

where R is the radius of the droplet and J_{TOT} is the total evaporation rate per unit length of the cylindrical line given by:

$$J_{TOT}(t) = \frac{2RJ_0\theta_c(t)}{\sin \theta_c(t)} \quad (5)$$

Figure 1b shows the predicted velocity distribution in the same cylindrical droplet drying with pinned contact area at two subsequent times where the initial contact angle of 30° falls to 15°. The arrows representing the flow field converging to the droplet edges, suggesting that an entrained nanostructure could be aligned by the flow and positioned at the narrow interface between the air, solvent, and substrate.

In this work, we ask if this internal flow in a cylindrical droplet can align and place anisotropic nanoparticles such as nanotubes or nanowires with precision on the nanometer scale. As a technological objective, the controlled parallel alignment and positioning of individual (unbundled) SWNT, for example, has not been demonstrated to date. To answer this question, we develop an experimental platform for creating cylindrical droplets and studying their internal hydrodynamics during evaporation. Statistics are generated on the frequency of alignment and placement errors, with experimental results directly compared to flow field simulations. The success of such a scheme is shown to depend upon a careful balancing of particle convection and solvent evaporation time scales. Last, we demonstrate that this method can align and place SWNT over preformed electrodes for electrical testing of individual nanotubes.

Results and Discussion. To verify the hypothesis that the hydrodynamic flow pattern in evaporating droplets with pinned contact, cylindrical geometry, and size of few micrometers could align and place single anisotropic nanostructures (SWNT in this work), we developed conditions under which cylindrical droplets could be readily formed and studied. Here, a gold-coated silicon wafer is patterned with alternating rectangular strips of a polar (cystamine) and nonpolar (octadecanethiol, ODT) self-assembled monolayer using microcontact printing[35] with a PDMS stamp. The width of the strips are ~3.5 μm (polar SAM) and ~2.5 μm (nonpolar SAM), respectively (Figure 2a). These dimensions ultimately become the diameter and regular pitch of an array of cylindrical droplets of aspect ratio exceeding 1000.

Interestingly, pure deionized (DI) water is simply excluded from the entire region of hydrophobic and hydrophilic patterns (Supporting Information Figure S1), but the addition of 1 wt % sodium dodecyl sulfate (SDS) surfactant causes segregation of the liquid into cylindrical droplets that originate at apparently random points and propagate along their length. We presume that these points are where the liquid film reaches a critical height (as discussed below). These cylindrical droplets are formed only on the polar SAM region (Figure 2c). During drying under these conditions, the contact area of these droplets remains pinned to the polar region, potentially allowing for the internal flow field (Figure 1b) to form as discussed below.[36]

The solution of SWNT (1 wt % SDS in water) is deposited by either immersion of the substrate into it or by application of few drops to cover the surface forming a thin, homogeneous film (microscopic image in Figure 2b). As the film dries, its height should reach a critical value where the surface free energy is minimized by segregating into the desired cylindrical droplets on the polar SAM region (Figure 2c). Figure 2 shows both the microscopic images and schematics of the process over time. This process of transition from continuous surface of liquid film to cylindrical droplets begins from several points within the film and they propagate along the length rapidly. The contact area of the droplets remains constant as it dries with its edges pinned to the edges of the polar SAM (Figure 2c,d). The process terminates as the ends at the length of the cylindrical drop contract rapidly, leaving a solvent-free surface (Figure 2e,f). Cylindrical sections after formation remain for an average time of 1.5 s before complete evaporation due to the length contraction, as observed using real-time video microscopy (see video, Supporting Information).[37] Because the cylindrical droplets created in this way evaporate with pinned contact area, theoretically the flow field described above should evolve within its interior. The fast contraction along the length prevents the final contact angle from reaching the receding value and the contact area apparently remains pinned. As observed previously,[26,27] the switching of the evaporation mode (pinned to unpinned) occurs when the contact angle drops below its receding value. Additionally, the contraction along the length is slow enough that it allows most of the nanotubes to reach the droplet edges.[38]

SWNT that have been individually suspended (largely free from bundles) in a surfactant/water mixture are utilized as a model anisotropic nanoparticle to probe the interior hydrodynamics of these micrometer size (diameter ~3.5 μm) droplets. When cylindrical drops are created with such solutions, subsequent AFM topographic images taken after solvent evaporation reveal individual nanotubes that are highly aligned and positioned in very close proximity (within 300 nm) to the polar/nonpolar SAM interface (Figure 3). We note that the parallel placement of individual (unbundled) nanotubes at pre-defined locations has not been achieved

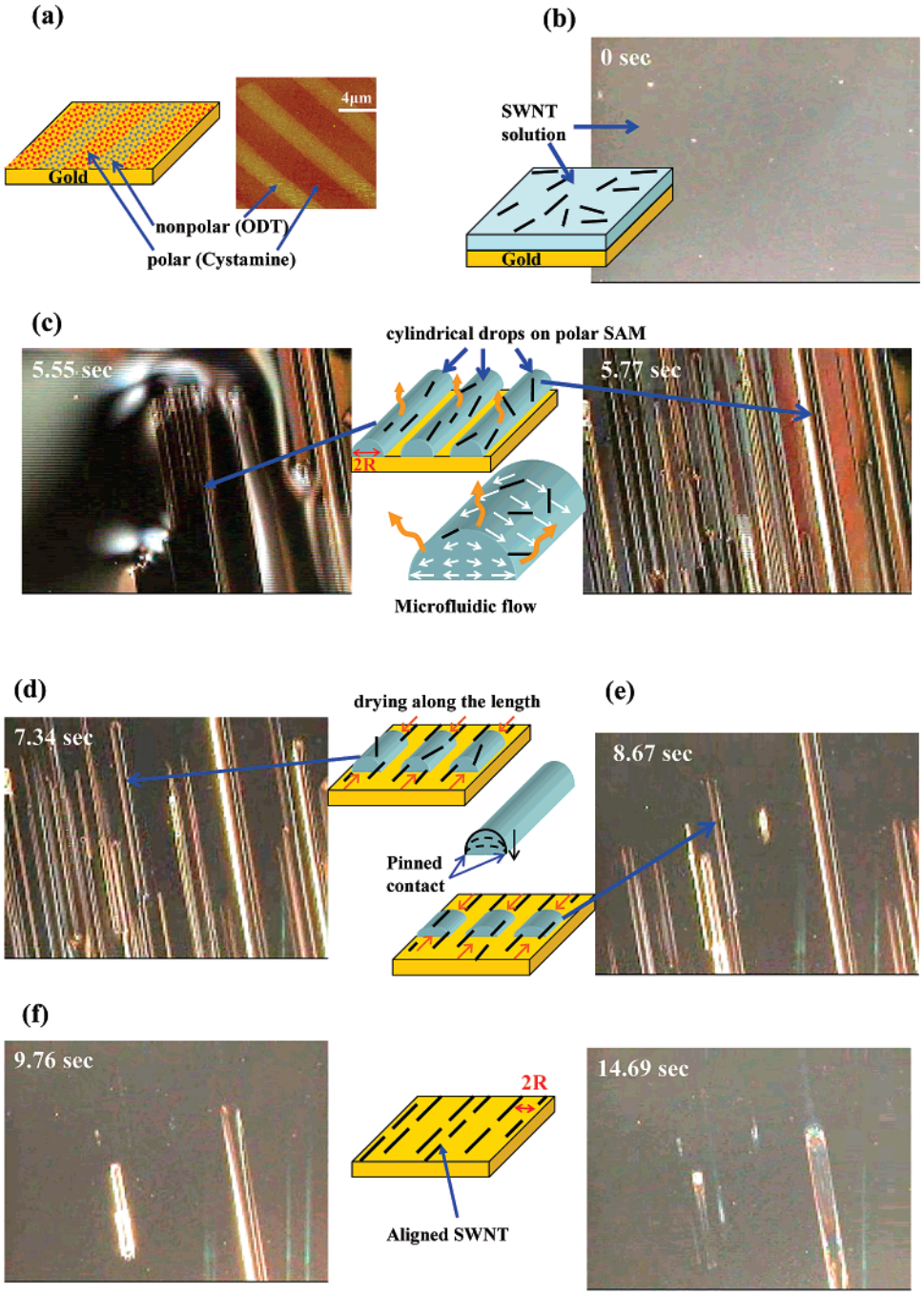

Figure 2. Microscopic images and schematics of SWNT alignment and placement using evaporation from micrometer sized cylindrical droplets. (a) Microcontact printing is used to create rectangular polar regions flanked by rectangular nonpolar domains (as shown by the AFM topography) each of width ~3.5 μm and ~2.5 μm, respectively, on gold surface over a length of 10 mm. (b) Initially, when SWNT solution is deposited on the gold surface, a thin liquid layer results with decreasing thickness due to evaporation. (c) At a critical height of the liquid film, the surface free energy is minimized by segregating into cylindrical droplets (~3.5 μm diameter). These cylinders are formed only in the polar SAM region. (d) As the cylindrical droplets dry, the contact area of these cylinders remains pinned to the width of polar pattern with decreasing contact angle. This drying process establishes a radial flow field within the drop pushing the entrained SWNT to the outermost edge of the polar SAM and aligning them before deposition. (e) The process terminates as the ends of the cylindrical droplets contracts rapidly (cylindrical section of ~3.5μm (2*R*) diameter remain for ~1.5 s) leaving a solution-free surface with deposited aligned SWNT on the edges of the polar SAM. (f) Drops that have a larger diameter (more than three times, 6*R*) than the droplets with average diameter of ~3.5 μm take a longer time to evaporate. Hence they can be seen on the surface even after most of the droplets have dried. This is the case when droplet is formed with its contact area on two polar patterns rather than one (including one or more polar/nonpolar pattern in between). (All the microscopic images are 223× magnified)

before. The number density at the interface increases with solution concentration (from Figure 3a−e) as expected, and continuous "wires" of nanotubes can be created using a concentration of 9.7 mg/L (Figure 3e). Section analysis on a statistically significant population of deposited SWNT confirms that they remain unbundled when deposited using this process. The inset to Figure 3b shows a nanotube height near 1 nm, corresponding to the diameter of a single electric

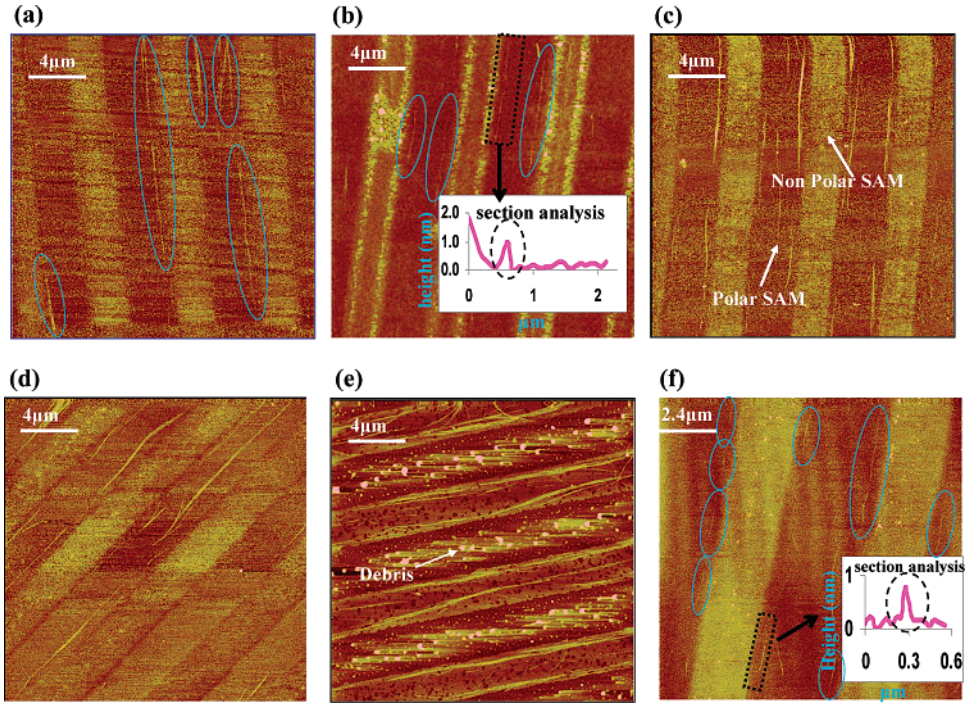

Figure 3. AFM topographic images showing alignment and placement of individual SWNT along the edges of the polar SAM (ovals highlight SWNT). (a) Highly aligned SWNT with low coverage for 4.6 mg/L concentration SWNT solution. (b) Inset is the section analysis of the area in the dotted region demonstrating deposition of individual SWNT (height ~1 nm). (c) Moderate coverage for 6.2 mg/L SWNT solution. Few SWNT along the center of the polar SAM and (d) at an offset from the edges of the polar SAM (error in perfect placement). (e) High coverage of SWNT resembling continuous wires of nanotubes for 9.73 mg/L SWNT solution. (f) Alignment of short individual SWNT (HiPco, average length ~0.8 μm). SWNT in (a−e) are electric arc synthesized (average length ~2.5 μm).

arc synthesized SWNT. Few small bundles (~2 nanotubes) can be seen in Figure 3c−e. We attribute this to the bundles already present in the solution due to insufficient ultracentrifugation (2 h at 30,000 RPM). This hydrodynamic deposition is observed not only for long SWNT (electric arc, average length ~ 2.5 μm) (Figure 3a−e), but also for shorter SWNT (HiPco, average length ~ 0.8 μm) (Figure 3f). In compiling several AFM topographic images, we observed some placement errors (Figure 3c,d), where positioning or alignment deviated from the typical observations (Figure 3a,b,f) although these were rare (statistics appear below). These errors generally include SWNT lying along the center of polar SAM or an offset ($\Delta x/R \sim 0.1-0.15$) from its edge. Last, using this technique, there is no control or correlation as to where the SWNT deposits along the linear interface. However, several features are reproduced fairly reliably: accurate positioning at an offset ($\Delta x/R \sim 0.1-0.15$) from the interface, excellent parallel alignment to the long axis of the cylindrical droplet, and preservation of individual SWNT in cases of both long and short nanotubes.

A simple model can be developed to capture the above observations. Consider a cylindrical droplet of diameter $2R \sim 3.5$ μm with entrained anisotropic nanoparticles (Figure 1a). Using the predicted velocity field (eq 1) in a cylindrical drying drop, the trajectory of a massless body (Figure 4 d,e) can be solved by integrating the transient field that evolves as the free surface of the drop moves downward with pinned contact drying. The resulting placement depends both on the initial position of the massless probe in this field and on the final contact angle. The final contact angle is defined as the angle when the drop vanishes due to contraction along the length. Figure 1b is the scaled velocity distribution predicted for a starting contact angle of 30°. As the droplet evaporates, the contact angle decreases and the free surface moves downward, but the flow field retains its orientation toward the periphery,[39] as shown for a later time when the contact angle reduces to 15°.

The experimental results can be directly compared with trajectories from flow field simulations. Compiling the exact position and orientation of over 372 SWNT from 20 AFM images produces a histogram of the position of the deposited SWNT from the interface of the polar/nonpolar SAM (Figure 4b). The vast majority of deposited SWNT reside near 0.85−1 times the cylinder radius (R) from the centerline (defined as $r = 0$, Figure 4a), with some deposition errors near the centerline of the polar SAM that are addressed below. The error in alignment angle can be compiled by defining $\text{ø} = 0°$ as a perfectly oriented SWNT lying parallel to the interface (Figure 4a). The same experimental data set shows nearly a negligible error in alignment at 0°, and it was therefore deemed unnecessary to simulate this variable (Figure 4c).

To simulate the statistical deviations in positioning, the transient quasistatic flow field was simulated by using eq 1. At constant evaporation flux, the height of the free surface and contact angle decrease according to eqs 3 and 4, respectively, and the resulting trajectories of massless probes which have been equally distributed in the droplet cross-section can be found by integration of this transient field. For probe particles with varying initial position, the final

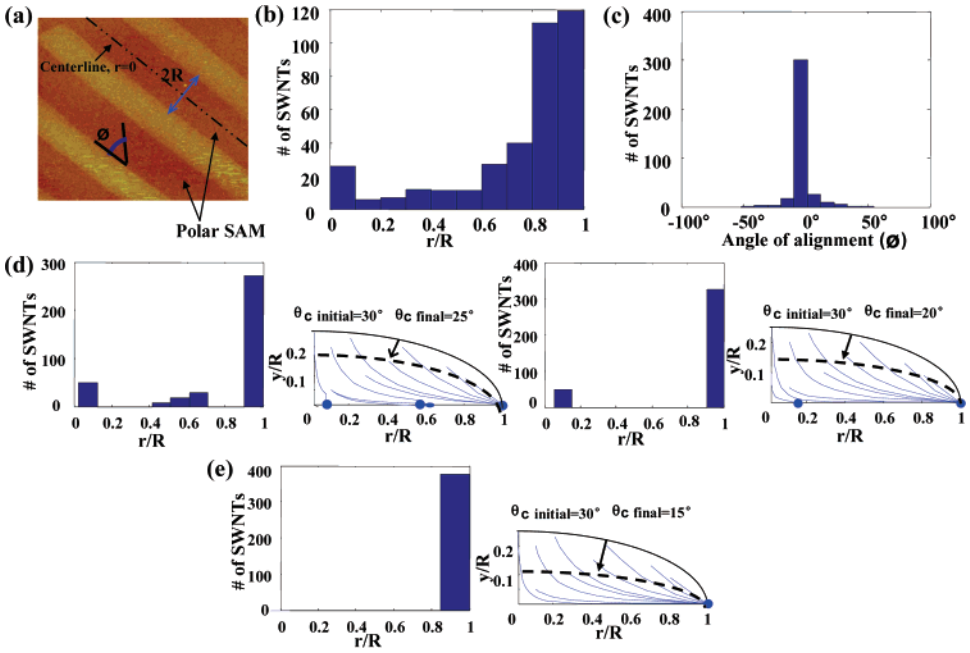

Figure 4. Comparison of experimental results with the continuum hydrodynamic modeling. (a) Width of the polar SAM is the diameter of the cylindrical droplets ($2R$) that have their center along the centerline ($r = 0$) of the polar SAM, ø is the angle of alignment. Experimental data compiled for 372 SWNT from 20 AFM images, with (b) the resulting placement with reference to the center line as $r/R = 0$ and (c) parallel alignment with reference ø as zero for SWNT parallel to the SAM edges. (d) Simulated statistical deviations in placement obtained by calculating the trajectories of massless probes in flow field of drying cylindrical droplet. Accuracy of deposition is a function of total deposition time (or final contact angle). If an initial contact angle of 30° decreases to 25° or 20°, the resulting histogram shows some placement errors with similarities to experimental data in (b). Note the small population near the center line is due to very low velocities in the region close to the axis. (e) If the droplet survives for longer times to decrease the contact angle below 15°, then a monodisperse placement results at the polar SAM edges. (Note: The *y*-axis is not in scale with the *x*-axis)

placement was recorded as that point where the trajectory ended when the final contact angle was reached (i.e., angle when the drop vanishes due to shrinkage along the length). Most of the particles reach the substrate much faster than those starting near the center ($r/R < 0.1$). We assumed that particles that do not reach the substrate ($y = 0$) before droplet evaporation end up at a point vertically translated downward when the final contact angle was reached. We find that the variation in the placement is a function of the starting contact angle and the total deposition time (or the final contact angle). For a rapid time to complete evaporation, or small change in contact angle, the droplet collapses before particles located near the centerline can translate to the edge. Figure 4 d,e plots trajectories of several massless probe particles starting at different locations within a cylindrical drop of initial contact angle 30°. If the process terminates at 25° or 20° (Figure 4d), the simulated histogram shows some placement errors at small r (close to the drop center). If the process terminates at longer time (Figure 4e), with 15° as final contact angle, the placement is perfect, with all the particles reaching the droplet edge ($r/R = 1$) as inferred from the simulated histogram. The center of the droplet has a stagnation point at $r/R = 0$, region of low velocity for $r/R < 0.1$, and placement errors normally result from particles initially placed here. Future efforts will examine alignment placement along the patterned regions systematically with the goal of achieving complete control on positioning.

We note an important distinction between this hydrodynamic method of alignment and placement and that of other self-assembly methods examined in the literature.[14−16] SWNT wrapped with anionic surfactant have no chemical affinity for the surface and will not deposit on a polar SAM under equilibrium conditions (immersing the substrate patterned with polar and nonpolar SAM in SWNT solution followed by rinsing in the solvent). Several recent studies have explored the equilibrium deposition of SWNT for patterning on a surface.[14−16] In this case, the particle interacts directly with chemical moieties on the surface, resulting in adhesion.[40] This restricts these methods to organic solvents in practicality and, invariably, to less-useful bundles of SWNT (Supporting Information Figure S2). In contrast, the microhydrodynamic method of alignment and placement should be operative for particles independent of their surface chemistry.

We show that this method can be used to position, align, deposit, and electrically connect individual (unbundled) SWNT over pre-patterned Au electrodes. It is noteworthy that this has not been achieved to date using other strategies for solution-based SWNT. We use a similar patterning approach as discussed above to create cylindrical droplets over 600 nm channel electrodes, resulting in individual nanotubes spanning the gap. Electrode pairs 20 μm wide with SAM pattern (Figure 2a) resulting in ~3.5 μm diameter patterned cylindrical droplets (~2.5 μm pitch) typically show two or more individual SWNT spanning the electrode gaps (Figure 5 a) at 6 mg/L SWNT solution concentration. AFM section analysis confirms that the connected SWNT are indeed individual and isolated. Remarkably, with no additional processing (i.e., annealing, subsequent lithography,

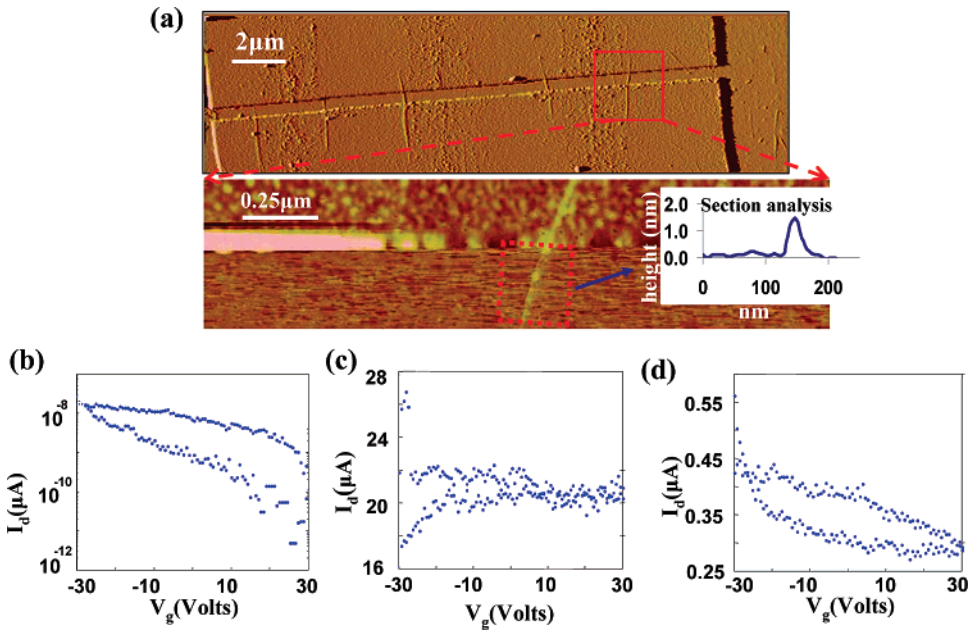

Figure 5. Demonstration that the technique can align, place and electrically contact SWNT over pre-patterned Au electrodes forming SWNT devices with individual and parallel SWNT bridging electrode gaps. Microhydrodynamic forces in a cylindrical droplet have been utilized to align and place individual SWNT over patterned electrodes from solution, forming electrically connected nanotubes without subsequent processing. Au electrodes are 20 μm in width with 600 nm channel length. (a) AFM image (amplitude) showing parallel SWNT bridging the electrode gap on almost all polar SAM edges with the AFM section analysis in the inset (topography image) demonstrating height of a single SWNT. (b−d) The contacted SWNT on such devices show electrical conductance, with measurable $I_d-V_d-V_g$ characteristics without any additional processing such as annealing or selective breakdown of metallic SWNT. (b) Contacted SC (on/off ratio >100), (c) metallic (no variation in I_d with V_g), and (d) both SC and metallic SWNT (on/off ratio ~2) are observed from the electrical testing.

metal sputtering, selective etching, or breakdown of metallic nanotubes) SWNT were electrically characterized and readily identified as having either metallic or semiconducting behavior. While contact resistance remains large due to the SAM interface between the SWNT and Au, we observe essentially three types of electrical responses from Current (I_d) versus gate voltage (V_g) characteristics: one with significant V_g-I_d modulation and high on−off ratio (~100) (Figure 5b), indicating only semiconducting (SC) nanotubes, a second type with negligible or no V_g-I_d modulation (Figure 5c), indicating only metallic nanotubes, and a third with a much lower on−off ratio (~2−10) indicative of both SC and metallic (Figure 5d). The trapping of single (unbundled) nanotubes across the gap significantly reduced the number of the third type. We anticipate that similar methods will lead to rapid and high throughput electrical screening of a given SWNT ensemble, enabling a clear determination of the number of semiconductors and metals in a given formulation.

Conclusions. We demonstrate that the hydrodynamic flow in a micrometer scale cylindrical drop evaporating with pinned contacts can align, position, and place both long (~2.5 μm) and short (~0.8 μm) single-walled carbon nanotubes (SWNT) with great accuracy. The potential flow model for a cylindrical droplet successfully explains the accuracy observed in the positioning of SWNT. As an application, the process was used for the top-down parallel alignment and placement of individual SWNT from solution. SWNT bridging up the gap are free from nanotube−nanotube junction/crossing and bundles. Because of the high accuracy in parallel alignment and placement, this technique looks promising for production of devices such as field effect transistors (FETs) and interconnects on a large scale from solution-based SWNT.

Method. *SWNT Solution Preparation.* Electric arc synthesized SWNT and HiPco SWNT (batch HPR 107.1) were suspended in 1 wt % sodium dodecyl sulfate (SDS) in DI water by 10 min sonication, followed by 2−5 h centrifugation at 30 000 RPM. Different centrifugation time resulted in different concentrations of the SWNT solution.

Substrate and Device Preparation. Gold-coated substrates were prepared by thermally depositing a 5 nm thick titanium layer, followed by a 50 nm Au deposition on a thermally oxidized Silicon wafer (600 nm SiO_2, Montco Silicon Technologies) under a high vacuum. Gold electrodes with 600 nm gap and 20 μm width were patterned on a thermally oxidized Si wafer (100 nm SiO_2) by e-beam lithography.

SWNT Deposition Process. Microcontact printing was used to form alternating SAMs of ODT molecules on Au surfaces.[35] This was followed by immersion in 2 mM cystamine solution in ethanol to form the polar SAM. This patterned substrate with alternating rectangular polar and nonpolar SAM was immersed in the SWNT solution (1 wt % SDS) for 1−2 s or a few drops of solution are applied on it with a pipet leading to a formation of thin, uniform liquid film. This film is left to dry in open air, followed by rinsing with copious amount of DI water to remove surfactant after

complete drying. Rinsing with water was done to remove the surfactant.

Microscopic Analysis. The movie and microscopic images of the process were taken at a magnification of 223×. Dimension 3100 (Digital instruments) was used for AFM imaging. Section analysis (a line profile on the surface of the SWNT) on topographic images was performed to determine the SWNT height. This refers to the measurement coming from a line profile on the surface of the SWNT.

Acknowledgment. This work was funded by an NSF Career award, a Beckman Young Investigator award, and a 3M Untenured Faculty Award to M.S.S., as well as from AFOSR grant (af fa 9550-06-1-0) and a Class A grant from Intel. AFM analysis was carried out in the Center for Microanalysis of Materials, University of Illinois, which is partially supported by the U.S. Department of Energy under grant DEFG02-91-ER45439. We thank Intel for providing the e-beam electrodes. We also acknowledge Paul Barone and Rachel Graff for useful discussions. Author contributions: M. Strano and R. Sharma designed and carried out all of the experiments and calculations. C.Y. Lee contributed in helping R. Sharma to make SAMs on gold as done by researchers before. J.H. Choi contributed useful discussions. K. Chen helped R. Sharma in the calculations. The paper was written by M. Strano and R. Sharma.

Supporting Information Available: Pure DI water on patterned surface. AFM topography images of equilibrium deposition of SWNT. Simulated statistical deviations in placement for 60° as initial contact angle. Video of the contact area of the droplets (MPEG). This material is available free of charge via the Internet at http://pubs.acs.org.

References

(1) Javey, A.; Guo, J.; Wang, Q.; Lundstrom, M.; Dai, H. J. *Nature* **2003**, *424*, 654−657.
(2) Naeemi, A.; Meindl, J. D. *IEEE Trans. Electron Devices* **2007**, *54*, 26−37.
(3) Kong, J.; Franklin, N. R.; Zhou, C. W.; Chapline, M. G.; Peng, S.; Cho, K. J.; Dai, H. J. *Science* **2000**, *287*, 622−625.
(4) Staii, C.; Johnson, A. T. *Nano Lett.* **2005**, *5*, 1774−1778.
(5) Snow, E. S.; Perkins, F. K.; Houser, E. J.; Badescu, S. C.; Reinecke, T. L. *Science* **2005**, *307*, 1942−1945.
(6) Bekyarova, E.; Davis, M.; Burch, T.; Itkis, M. E.; Zhao, B.; Sunshine, S.; Haddon, R. C. *J. Phys. Chem. B* **2004**, *108*, 19717−19720.
(7) Misewich, J. A.; Martel, R.; Avouris, P.; Tsang, J. C.; Heinze, S.; Tersoff, J. *Science* **2003**, *300*, 783−786.
(8) Chen, X. Q.; Saito, T.; Yamada, H.; Matsushige, K. *Appl. Phys. Lett.* **2001**, *78*, 3714−3716.
(9) Krupke, R.; Hennrich, F.; Weber, H. B.; Kappes, M. M.; von Lohneysen, H. *Nano Lett.* **2003**, *3*, 1019−1023.
(10) Xin, H. J.; Woolley, A. T. *Nano Lett.* **2004**, *4*, 1481−1484.
(11) Smith, B. W.; Benes, Z.; Luzzi, D. E.; Fischer, J. E.; Walters, D. A.; Casavant, M. J.; Schmidt, J.; Smalley, R. E. *Appl. Phys. Lett.* **2000**, *77*, 663−665.
(12) O'Shea, J. N.; Taylor, J. B.; Swarbrick, J. C.; Magnano, G.; Mayor, L. C.; Schulte, K. *Nanotechnology* **2007**, *18*, 035707.
(13) McLean, R. S.; Huang, X. Y.; Khripin, C.; Jagota, A.; Zheng, M. *Nano Lett.* **2006**, *6*, 55−60.
(14) Rao, S. G.; Huang, L.; Setyawan, W.; Hong, S. H. *Nature* **2003**, *425*, 36−37.
(15) Lee, M.; Im, J.; Lee, B. Y.; Myung, S.; Kang, J.; Huang, L.; Kwon, Y. K.; Hong, S. *Nat. Nanotechnol.* **2006**, *1*, 66−71.
(16) Wang, Y.; Maspoch, D.; Zou, S.; Schatz, G. C.; Smalley, R. E.; Mirkin, C. A. *Proc. Natl. Acad. Sci. U.S.A.* **2006**, *103*, 2026−2031.
(17) Zheng, M.; Jagota, A.; Semke, E. D.; Diner, B. A.; McLean, R. S.; Lustig, S. R.; Richardson, R. E.; Tassi, N. G. *Nat. Mater.* **2003**, *2*, 338−342.
(18) It is known that individual nanotubes can be suspended in organic solvent with extensive functionalization (Liang, F.; Sadana, A. K.; Peera, A.; Chattopadhyay, J.; Gu, J.; Hauge, R. H.; Billups, W. E. *Nano Lett.* **2004**, *4*, 1257−1260). Such heavily functionalized SWNT have limited utility for electronic applications and historically have been excluded from studies of device fabrication from solution processing. It is also uncertain if the functionalized nanotubes will show a similar interaction with the patterned SAM on surface.
(19) Cao, Q.; Hur, S.-H.; Zhu, Z.-T.; Sun, Y. G.; Wang, C.-J.; Meitl, M. A.; Shim, M.; Rogers, J. A. *Adv. Mater.* **2006**, *18*, 304−309.
(20) Kocabas, C.; Shim, M.; Rogers, J. A. *J. Am. Chem. Soc.* **2006**, *128*, 4540−4541.
(21) Duggal, R.; Hussain, F.; Pasquali, M. *Adv. Mater.* **2006**, *18*, 29−34.
(22) Naeemi, A.; Sarvari, R.; Meindl, J. D. *IEEE Electron Device Lett.* **2005**, *26*, 84−86.
(23) Picknett, R. G.; Bexon, R. *J. Colloid Interface Sci.* **1977**, *61*, 336−350.
(24) Cachile, M.; Benichou, O.; Cazabat, A. M. *Langmuir* **2002**, *18*, 7985−7990.
(25) Dugas, V.; Broutin, J.; Souteyrand, E. *Langmuir* **2005**, *21*, 9130−9136.
(26) Yu, H. Z.; Soolaman, D. M.; Rowe, A. W.; Banks, J. T. *ChemPhysChem* **2004**, *5*, 1035−1038.
(27) Erbil, H. Y.; McHale, G.; Rowan, S. M.; Newton, M. I. *Langmuir* **1999**, *15*, 7378−7385.
(28) Deegan, R. D.; Bakajin, O.; Dupont, T. F.; Huber, G.; Nagel, S. R.; Witten, T. A. *Nature* **1997**, *389*, 827−829.
(29) Deegan, R. D.; Bakajin, O.; Dupont, T. F.; Huber, G.; Nagel, S. R.; Witten, T. A. *Phys. Rev. E* **2000**, *62*, 756−765.
(30) Petsi, A. J.; Burganos, V. N. *Phys. Rev. E* **2005**, *72*, 047301.
(31) Petsi, A. J.; Burganos, V. N. *Phys. Rev. E* **2006**, *73*, 041201.
(32) Kimura, M.; Misner, M. J.; Xu, T.; Kim, S. H.; Russell, T. P. *Langmuir* **2003**, *19*, 9910−9913.
(33) Smalyukh, I. I.; Zribi, O. V.; Butler, J. C.; Lavrentovich, O. D.; Wong, G. C. L. *Phys. Rev. Lett.* **2006**, *96*, 177801.
(34) Bigioni, T. P.; Lin, X. M.; Nguyen, T. T.; Corwin, E. I.; Witten, T. A.; Jaeger, H. M. *Nat. Mater.* **2006**, *5*, 265−270.
(35) Xia, Y. N.; Mrksich, M.; Kim, E.; Whitesides, G. M. *J. Am. Chem. Soc.* **1995**, *117*, 9576−9577.
(36) We attribute the difference between pure water and water/surfactant mixture to the differences in their surface tension. Surface tension directly determines the contact angle of drops. The large value of surface tension of water leads to only large contact angle drops to form on this substrate. Small diameter drops of few micrometers with large contact angle might be highly unstable and hence unable to form. As a result, no drop formation takes place. However, surfactant significantly lowers the surface tension, leading to formation of smaller contact angle drops that are stable and hence are able to form.
(37) The cylinders that have a diameter ∼9.5 μm or higher take longer time (more than 3 s) to evaporate. These are the cylinders that are formed with contact area as two or more polar SAMs (including the nonpolar SAMs in between).
(38) Initially, when the droplet is formed, nanotubes are present more in number in the central region of the droplet, which is the same as the central region of the polar SAM due to higher volume of liquid there. Ultimately, the SWNT end up in the lower volume region of the droplet in which the SAM edges are the same as the droplet edges. This rules out the fact that fast contraction along the length would have led to alignment. If fast contraction along the length would have led to alignment, then aligned nanotubes should be present in the entire polar SAM region after evaporation.
(39) The actual value of the contact angle could not be estimated experimentally using goniometry because of the small dimensions of a few micrometers of the drop. Hence we did these calculations for a wide range (20−60°) of initial contact angles. Very similar results with slight variations were observed for them.
(40) To verify that SDS/SWNT have no direct affinity for the polar SAM, several experiments were conducted where the patterned wafer was immersed directly into a SWNT solution (1 wt % SDS in water) for 2 min, as is typically done for equilibrium deposition. Negligible or no adhesion was found.

NL0711211